Supplementary Materials

Revealing interfacial disorder of thick many-layer epitaxial graphene on SiC: a complementary neutron and x-ray scattering investigation

A.R. Mazza,[a] A.L. Miettinen,[b] A.A. Daykin,[a] X. He,[c,d] T.R. Charlton,[e] M. Conrad,[a] S. Guha,[b] Q. Lu,[a] G. Bian,[a] E.H. Conrad,[b] and P.F. Miceli*[a]

1 Raman Measurement of Graphene Thickness

We show that the graphene thickness can be reliably obtained from Raman intensities[1] and these compare accurately with the thicknesses obtained from x-ray reflectivity. Using an Invia Renishaw Raman spectrometer with a 514nm laser spot size of $2\mu m$ and power density $2.5\times10^4 W/cm^2$ in a confocal backscattered geometry, the SiC 2^{nd} order Raman peak at $1525cm^{-1}$ was measured on several samples. Because of the attenuation of light as it passes (twice) through each graphene layer, the Raman intensity is related to the number of graphene layers, N, according to eq.1.

$$I_{SiC}(N) = v^{2N} \tag{1}$$

where v is the transmission through one graphene layer ($v^2 = 0.955$)[2] and the intensity was normalized using a blank SiC reference sample. Fig. S1 shows excellent agreement with the XRR results where the Raman thickness is given as N multiplied by the interlayer spacing of graphene 3.37Å. These thicknesses were also found to agree with the thicknesses that we also measured by the attenuation of the Si signal in x-ray photoelectron spectroscopy (XPS). As compared to XPS, it is noted that the Raman measurements are quicker and easier to perform and are not as limited in depth (the absorption length of the Raman laser is larger than the soft x-rays used for the XPS measurements). Samples were also characterized using XPS after growth. Layer thicknesses were calculated using the shifted carbon emission spectrum peak intensities and the known attenuation length and atomic sensitivity factors for graphitic carbon and silicon carbide:

$$layers = l_g/t_g \times ln(1 + I_g/\alpha_g \times \alpha_{SiC}/I_{SiC}), \tag{2}$$

where l_g is the attenuation length of graphene, t_g is the graphene layer thickness, I_g and I_{SiC} are the C1s peak intensities of graphitic carbon and silicon carbide, α_g and α_{SiC} are the atomic sensitivity factor of graphitic carbon and silicon carbide respectively.

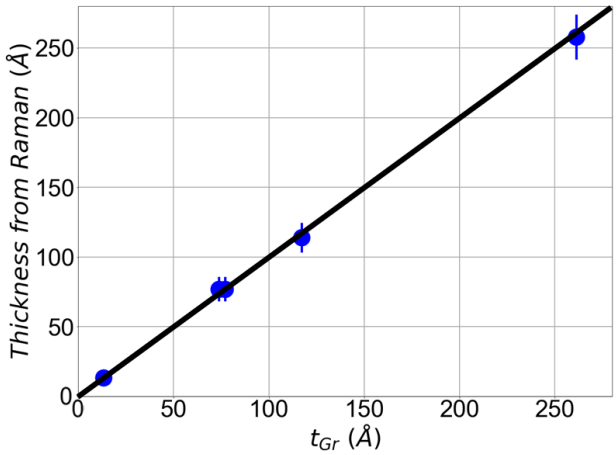

Fig. S 1 shows excellent agreement between the graphene thickness obtained from the SiC Raman intensity given in eq. 1 and that which was obtained by XRR (t_{Gr} from Tab. 1 of the main text).

2 Description of EXRR Modeling

Here we describe the details of the amplitudes appearing in eq.(1) of the main text, which result from the different layers shown in the schematic diagram of Fig. 7 in the main text. The first term represents the amplitude arising from the semi-infinite C-face 4H-SiC substrate whereas $A_G^B(l)$ and $A_G^T(l)$ are the amplitudes arising from the bottom and top graphene layers, respectively.

The amplitude of a graphene film is constructed from the basic form of the amplitude for a disordered thin film, as described elsewhere[3]:

$$A = \psi\frac{\xi - 1}{\psi - 1} \tag{3}$$

where ψ is an average phase factor $< e^{iqd} >_d$ from a distribution of interlayer spacings of graphene, d. Here, we will assume a Gaussian distribution of these spacings,

$$\psi = e^{-\frac{2(\pi l\Delta d)^2}{c_{SiC}^2}} e^{\frac{i2\pi ld}{c_{SiC}}} \tag{4}$$

where Δd is the width of the distribution of d-spacings. The fluctuation in the graphene film thickness is described by a binomial distribution of M discrete layers so that,

$$\xi = (\frac{N}{M}\psi + (1 - \frac{N}{M}))^M \tag{5}$$

where N is the average number of layers in the film and the vari-

[a] Department of Physics and Astronomy, University of Missouri, Columbia, Missouri, USA
[b] Georgia Institute of Technology, School of Physics, Atlanta, Georgia, USA
[c] Electron Microscopy Core, University of Missouri, Columbia, Missouri, USA
[d] Department of Mechanical and Aerospace Engineering, University of Missouri, Columbia, Missouri, USA
[e] Spallation Neutron Source, Oak Ridge National Laboratory, Oak Ridge, Tennessee, USA
* E-mail: micelip@missouri.edu

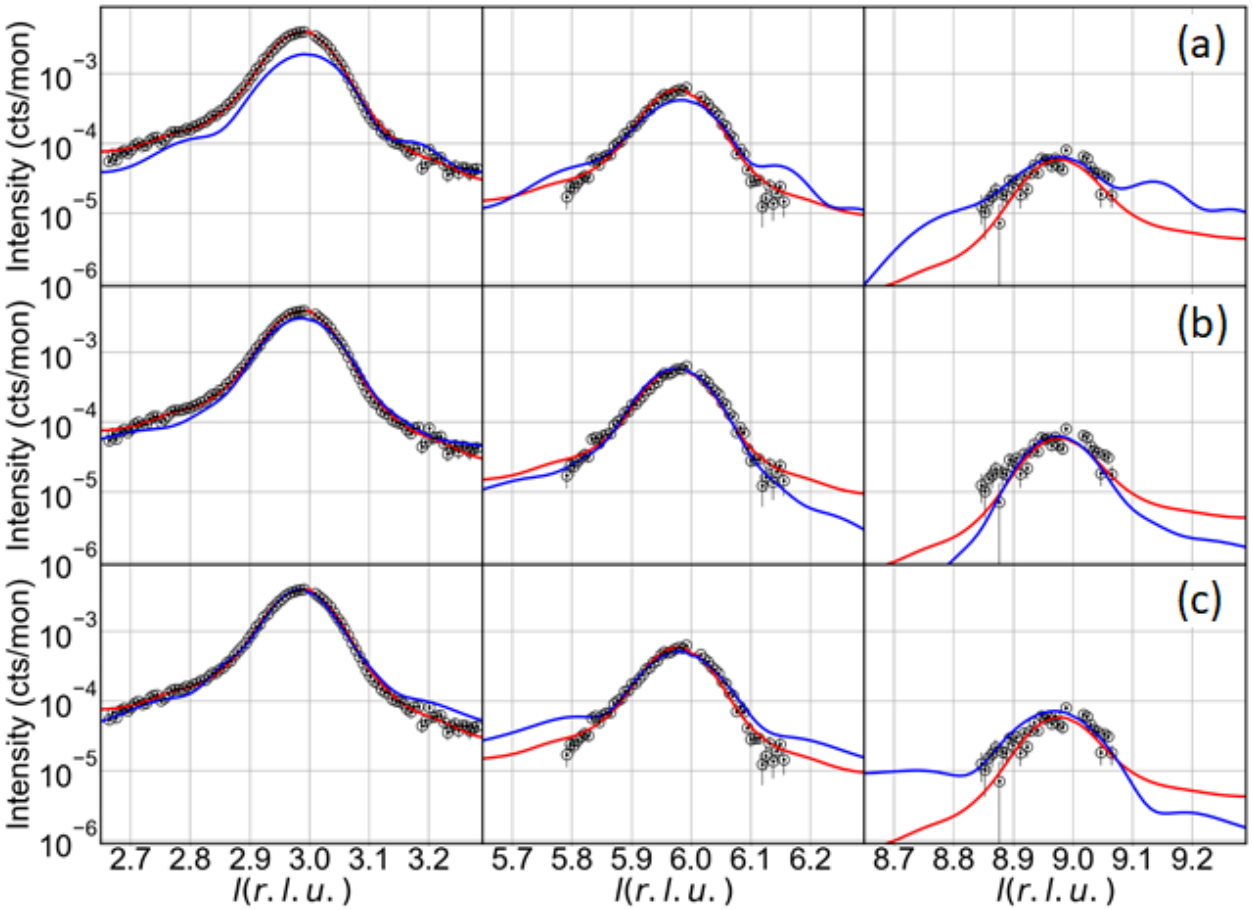

Fig. S 2 shows the best fit (red curves) for sample 33MO6 (symbols) compared to various constraints or modifications (blue curves) of the model that are associated with the graphene interlayer spacing. The first, second, and third order graphene reflections of the EXRR are shown from left to right in each of (a)-(c). (a) constrains $d^B_{Gr} = d^T_{Gr}$ and $\Delta d^B_{Gr} = \Delta d^T_{Gr}$; (b) constrains $d^B_{Gr} = d^T_{Gr}$ but $\Delta d^B \neq \Delta d^T$; and (c) switches the stacking of the layers so that the expanded layer is on top of the thicker layer.

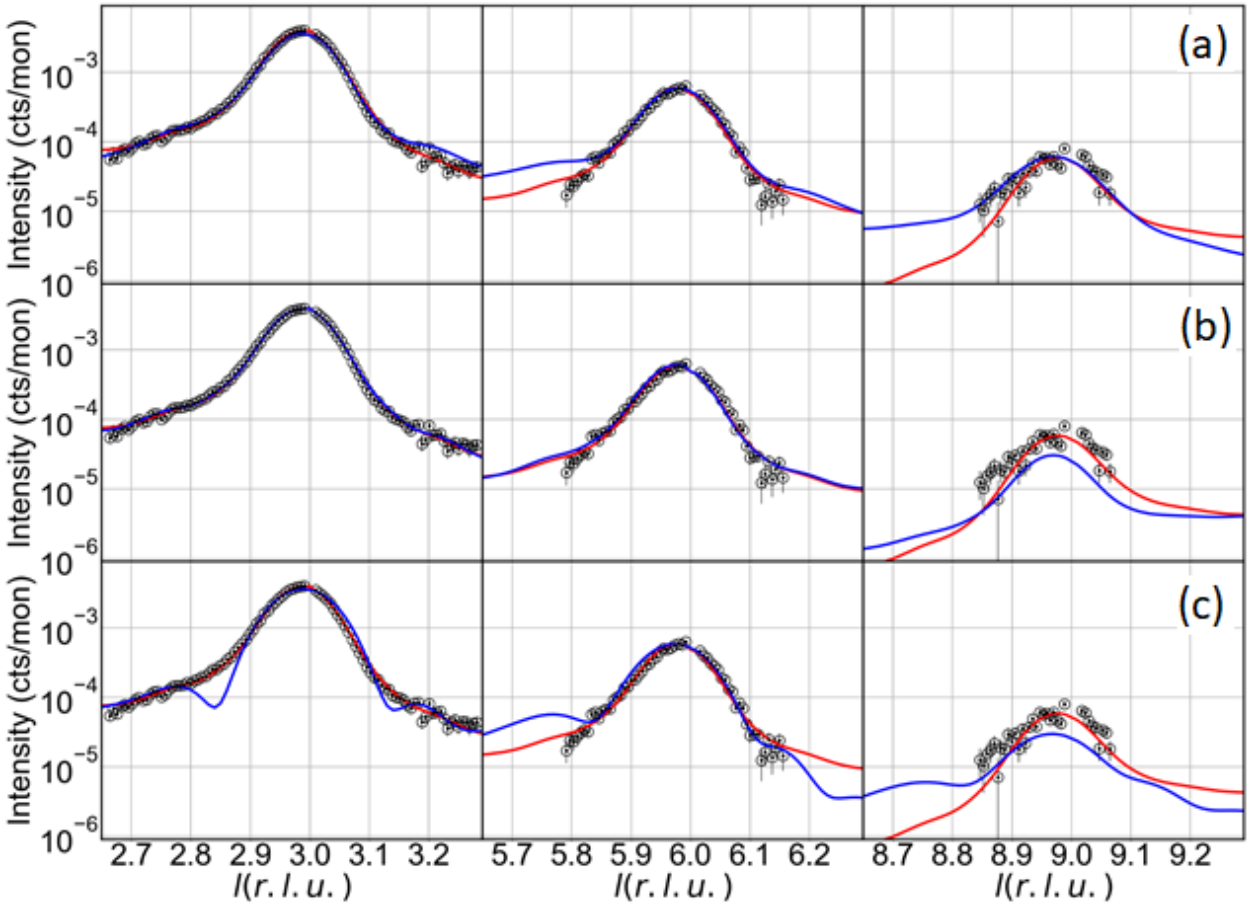

Fig. S 3 shows the best fit (red curves) for sample 33MO6 (symbols) compared to various constraints or modifications (blue curves) for the model that are associated with the graphene film thickness. The first, second, and third order graphene reflections of the EXRR are shown from left to right in each of (a)-(c). (a) requires the bottom and top layers to both start at the substrate rather than be vertically stacked; (b) does not allow for height variations in the bottom layer; and (c) only allows for a single distribution of heights in the top layer rather than three distributions.

ance of the layer height-distribution is given as $S^2 = N(1 - \frac{N}{M})$. In the present case, we find that the graphene films are in the Poisson limit where M tends to infinity and $S^2 = N$.

The amplitudes for the bottom and top graphene layers are then constructed from eq.(3) using $d = d^B_{Gr}$ or d^T_{Gr} and $\Delta d = \Delta d^B_{Gr}$ or Δd^T_{Gr} for the bottom and top graphene layers, respectively, for ψ and ξ. For the bottom graphene layer,

$$A^B_G(l) = e^{i2\pi l d^{1st}_{Gr}/c_{SiC}} f_c(l)(\psi_B \frac{\xi_B - 1}{\psi_B - 1}) \quad (6)$$

where $f_c(l)$ is the atomic form factor of carbon. d^{1st}_{Gr} accommodates the phase shift due to the distance of the first graphene layer from the substrate. Because our EXRR measurements had limited data in between the Bragg positions, our measurements were relatively insensitive to d^{1st}_{Gr}. This value was found to vary between $1.6 - 3$Å, giving a contraction in the first layer that is consistent with other studies[4].

The top layer was constructed similarly except that a larger film thickness fluctuation was required and we used a weighted average of three distributions of graphene layers,

$$A^T_G(l) = e^{i2\pi l d^{1st}_{Gr}/c_{SiC}} f_c(l)\xi_B\psi_T\Sigma^3_{n=1} g_n \frac{\xi_n - 1}{\psi_T - 1} \quad (7)$$

where g_n describes the weighting of the distributions subject to $\Sigma^3_{n=1} g_n = 1$. ξ_n depends on one of three possible layer heights, N_n, with $n = 1,2,3$. The average total thickness of the graphene film is $\overline{N} = N_B + \Sigma^3_{n=1} g_n N^n_T$ and it is reported in Table 3 of the main text. Because of the Poisson limit, $\overline{N}$ is also the total variance so that the graphene roughness is given as $\sigma_{EXRR} = \sqrt{\overline{N}}d$.

All parameters in the model were allowed to refine using non-linear least squares fitting. The resulting fits for three samples are represented by the red lines in the plots in Fig. 6 of the main text. In the analysis, Δd played an important role, both in diminishing intensity oscillations at the graphene Bragg reflections as well as in accounting for the intensity ratios between different orders of reflections. Careful consideration of each of the parameters of the model was required and these are explored in Figs. S2 and S3, where the need for these parameters were studied by applying constraints to the model and comparing to the best fit for sample 33MO6.

To explore the necessity of having a bottom graphene layer that is different than the top, a fit without a difference in these layers is shown in Fig. S2(a). Here ratio of intensities among different orders of reflection cannot follow the measured values while there are oscillations (fringes) that are too large in amplitude. In Fig. S2(b) it can be seen that allowing the Δd of the two layers to be different (while still requiring their d values to be the same) makes a significant improvement in the quality of fit. However, further significant improvement (red curve in Fig. S2(b)) is obtained by allowing the presence of a thin and slightly expanded graphene layer that accommodates the intensity shoulder towards lower q.

We also determined that the expanded thin graphene layer appears at the bottom rather than on the top of the thicker graphene layer. Fig. S2(c) shows that if the thin expanded layer is on the top, there is an overestimation of intensity in the tails of the Bragg reflections. This problem does not occur when the thin layer is on the bottom because $\Delta d^B_{Gr} > \Delta d^T_{Gr}$ allows for a greater attenuation of the top layer intensity arising from the factor ξ_B in eq. (7).

We determined that the thin and thick graphene layers cannot be laterally located next to each other, with both starting at the substrate rather than being vertically stacked as in Fig. 7 of the main manuscript. This case is shown in Fig. S3(a) where, similar to what occurs in Fig. S2(c), there is too much intensity in the tails of the Bragg reflections because of the lack of attenuation coming from ξ_B (with $\Delta d^B_{Gr} > \Delta d^T_{Gr}$) that would now be absent from eq. (7).

Correctly describing the height distributions of the graphene layers was vital for capturing the shape of the graphene Bragg reflections. Fig. S3(b) shows a fit with a perfectly uniform ($N = M$) bottom layer while maintaining the height distribution of the top layer obtained from a best fit. While this seems to work for the low order reflections, the third order intensity is significantly in error and the effect of having a smooth interface between the bottom and top layers is more subtle. In turns out that in order to compensate for a smooth interface in the bottom layer, the modified fit (blue curve) required larger Δd^B_{Gr} (it also affects peak shape) in the bottom layer which then causes too much attenuation at the higher order Bragg reflections. A good fit (red curve) was obtained in the Poisson limt ($M >> N$) so that the bottom layer roughness is given by $\sigma_B = \sqrt{N^B}d$.

The height distribution of the top graphene layer plays a dominant role in the shape of the Bragg reflections. In Fig. S3(c) the importance of multiple height distributions in fitting the data is demonstrated, where it can be seen that a single Poisson distribution cannot adequately describe the data. In particular, strong oscillations occur in the model that are not present in the data. Using three distributions, as given in eq. (7), removes these oscillations.

Acknowledgements

This research was supported by the National Science Foundation under Grant No. DGE-1069091, Oak Ridge National Lab's Graduate Opportunities! Program, and by the Department of Energy (DOE) Office of Science Graduate Student Research. A portion of this research used resources at the Spallation Neutron Source, a DOE Office of Science User Facility operated by the Oak Ridge National Laboratory. The TEM work was supported by the University of Missouri Electron Microscopy Core Excellence in Electron Microscopy award.

Notes and references

1 S. Shivaraman, M. V. S. Chandrashekhar, J. J. Boeckl and M. G. Spencer, *Journal of Electronic Materials*, 2009, **38**, 725–730.

2 S.-E. Zhu, S. Yuan and G. C. A. M. Janssen, *EPL (Europhysics Letters)*, 2014, **108**, 17007.

3 P. Miceli, *Semiconductor Interfaces, Microstructures and Devices: Properties and Applications*, IOP Publishing, Bristol, 1993, pp. 87–110.

4 J. Hass, J. E. MillÃąn-Otoya, P. N. First and E. H. Conrad, *Physical Review B*, 2008, **78**, 1–10.